Ground-based FTIR retrievals of SF$_6$ at Réunion Island

Minqiang Zhou[1,2,3], Bavo Langerock[2], Corinne Vigouroux[2], Pucai Wang[1,3], Christian Hermans[2], Gabriele Stiller[4], Kaley A. Walker[5], Geoff Dutton[6], Emmanuel Mahieu[7], and Martine De Mazière[2]

[1]Key Laboratory of Middle Atmosphere and Global Environment Observation, Institute of Atmospheric Physics, Chinese Academy of Sciences, Beijing, China
[2]Royal Belgian Institute for Space Aeronomy (BIRA-IASB), Brussels, Belgium
[3]University of Chinese Academy of Sciences, Beijing, China
[4]Karlsruhe Institute of Technology, Karlsruhe, Germany
[5]University of Toronto,Toronto, Canada
[6]Earth System Research Laboratory, NOAA, Boulder, Colorado, USA
[7]Institut d'Astrophysique et de Géophysique, Université de Liège, Liège, Belgium

Correspondence to: Minqiang Zhou (minqiang.zhou@aeronomie.be)

Abstract. SF$_6$ total columns were successfully retrieved from FTIR measurements (Saint Denis and Maïdo) at Réunion Island (21°S, 55°E) between 2004-2016 using the SFIT4 algorithm: the retrieval strategy and the error budget were presented. The FTIR SF$_6$ retrieval has independent information in only one individual layer, covering the whole troposphere and the lower stratosphere. The trend of SF$_6$ was analysed based on the FTIR retrieved dry air column-averaged mole fractions (X_{SF_6}) at
5　Réunion Island, the in-situ measurements at America Samoa (SMO) and the collocated satellite measurements (MIPAS and ACE-FTS) in the southern tropics. The SF$_6$ annual growth rate from FTIR retrievals is 0.265±0.013 pptv/year for 2004–2016, which is slightly weaker than that from the SMO in-situ measurements (0.285±0.002 pptv/year) for the same time period. The SF$_6$ trend in the troposphere from MIPAS and ACE-FTS observations is also close to the ones from the FTIR retrievals and the SMO in-situ measurements.

1 Introduction

Sulfur hexafluoride (SF$_6$) is very stable in the atmosphere and is one of the well-mixed most potent greenhouse gases listed in the 1997 Kyoto protocol linked to the United Nations Framework Convention on Climate Change (UNFCCC). It has an extremely long lifetime of 850 years (Ray et al., 2017) with Global Warming Potential for a 100-years time horizon of 23700 (relative to CO$_2$) (Kovács et al., 2017). Since SF$_6$ is very stable trace gas in the atmosphere and its annual growth rate seems
15　relatively constant during the last two decades (Hall et al., 2011), it is usually applied to calculate the age of air (Patra et al., 1997; Engel, 2002; Patra et al., 2009; Stiller et al., 2012; Haenel et al., 2015).

　　SF$_6$ is emitted from anthropogenic sources at the Earth's surface, mainly from the chemical industry, such as production of electrical insulators and semi-conductors, and magnesium manufacturing. The mole fraction of SF$_6$ in the atmosphere keeps increasing in recent years and the globally averaged near-surface SF$_6$ volume mixing ratio (VMR) has reached up to 7.6 pptv
20　(parts per trillion by volume), with an annual increase of 0.3 pptv/year in 2012 (WMO, 2014). Fig. 1 shows the SF$_6$ historical global emissions in 1900-2005 (Schultz et al., 2008; Mieville et al., 2010). Emissions of SF$_6$ started in the 1940′s and have been

increasing since then. Only during the 1990-2000′s the emissions almost remain constant. The most likely reason is that SF_6 emissions decreased in developed countries between 1995 and 1998, but then increased again after 1998 (Levin et al., 2010; Rigby et al., 2010). The SF_6 global total emissions in 2005 were 6.341 Gg/year (1 Gg = 1000 tons), which is about eight times larger than that in 1970 (0.789 Gg/year). Fig. 1 also shows the predictions of SF_6 global emissions for 2005-2100 according to four Representative Concentration Pathways (RCP) scenarios with different radiative forcing values (2.6, 4.5, 6.0 and 8.5 W/m^2) in 2100 relative to pre-industrial values (Moss et al., 2010). RCP 6.0 and RCP 8.5 scenarios assume the emissions keep increasing until 2020 and 2100 respectively, while RCP 2.6 and RCP 4.5 scenarios assume that there will be a steep decrease after 2010. The predictions from these 4 scenarios are very different, so that it is very important to monitor the abundance of SF_6 in the atmosphere. The most recent Scientific Assessment of Ozone Depletion report (WMO, 2014) points out that the global emissions have amounted to 8.0 Gg/year in 2012, marked by a black dot in Fig. 1.

The Advanced Global Atmospheric Gases Experiment (AGAGE) gas chromatographic-mass spectrometric (GC-MS) system has been applied to measure the SF_6 concentration since 1973 (Rigby et al., 2010). The Halocarbons and other Atmospheric Trace Species Group (HATS) started SF_6 sampling measurements at eight stations in 1995 and in-situ measurements at six fixed sites in 1998 (Hall et al., 2011). The flask and in-situ measurements show that the SF_6 abundance in the atmosphere has been increasing since the 1970s (Maiss and Levin, 1994; Geller et al., 1997; Maiss and Brenninkmeijer, 1998; Moss et al., 2010). In recent decades, remote sensing techniques also contribute to monitoring SF_6. Rinsland et al. (1990) used the spectra observed by the Atmospheric Trace MOlecule Spectroscopy instrument (ATMOS) aboard the space shuttle, as part of the Spacelab 3 (SL3) payload, to retrieve SF_6 concentrations in the upper troposphere and lower stratosphere. In addition, space-based sensors, such as the Atmospheric Chemistry Experiment–Fourier Transform Spectrometer (ACE-FTS) (Bernath et al., 2005; Bernath, 2017) and the Michelson Interferometer for Passive Atmospheric Sounding (MIPAS) (Stiller et al., 2008), are applied to obtain an SF_6 global distribution and trend. Zander et al. (1991) succeeded in monitoring the increasing total column of SF_6 using the ground-based Fourier transform infrared spectrometer (FTIR) at Jungfraujoch (46.55°N, 7.98°E, 3.58 km a.s.l.). Later on, Rinsland et al. (2003) and Krieg et al. (2005) obtained the total columns of SF_6 from the FTIR measurements at Kitt Peak (31.9°N, 111.6°W, 2.09 km a.s.l.) and Ny–Ålesund (78.91°N, 11.88°E, 0.02 km a.s.l.). They found that the mixing ratio of SF_6 is continuously increasing and that the mean increases of SF_6 is 0.31±0.08 pptv/year at Ny–Ålesund, 0.24±0.01 pptv/year at Jungfraujoch, and 0.28±0.09 pptv/year at Kitt Peak from March 1993 to March 2002. In the latest Scientific Assessment of Ozone Depletion, the trends of SF_6 from in-situ measurements are consistent with the trends in the troposphere from remote sensing measurements (ACE-FTS, MIPAS and Jungfraujoch FTIR) (WMO, 2014).

The objective of this paper is to investigate the SF_6 retrievals in the southern tropics based on the spectra observed by two FTIR spectrometers at Réunion Island (21°S, 55°E) from 2004 to 2016. In sect. 2, SF_6 retrievals are carried out with the well-established SFIT4 algorithm, which is upgraded from the radiative transfer and retrieval algorithm SFIT2 (Pougatchev et al., 1995; Hase et al., 2004) and widely used in the Network for the Detection of Atmospheric Composition Change-Infrared Working Group (NDACC-IRWG) community. The FTIR SF_6 retrieval strategy and the error budget are discussed in detail. In the following section, the trend of SF_6 is analysed based on the FTIR retrievals, the HATS America Samoa (SMO) in-

situ measurements (14°S, 170°W, 77 m a.s.l.) and the collocated satellite measurements (MIPAS and ACE-FTS). Finally, conclusions are drawn in Sect. 4.

2   FTIR retrievals at Réunion Island

The Royal Belgian Institute for Space Aeronomy operates two FTIR sites at Réunion Island. One is at Saint Denis (St Denis) close to the coast (20.90° S, 55.48° E; 85 m a.s.l.) and the other one is located at the Maïdo mountain site (21.07° S, 55.38° E; 2155 m a.s.l.). At present, both sites are equipped with a Bruker 125HR spectrometer, a precise solar-tracker system and an automatic weather station. The St Denis FTIR is dedicated to the near-infrared spectral region and contributes to the Total Carbon Column Observing Network (TCCON) since September 2011, whereas the Maïdo FTIR is dedicated to the mid- to thermal infrared spectral region and has become an NDACC-IRWG instrument in March 2013. Before September 2011, a Bruker 120M instrument was operated at St Denis in the NDACC mid- to thermal infrared configuration. For detailed information about the two sites, please refer to Zhou et al. (2016) and the references therein.

The SF_6 retrievals use the spectra in the thermal infrared range. Therefore, we select the spectra from the Bruker 120M at St Denis (2004-2011) and from the Bruker 125HR at Maïdo (2013-2016).

The spectra of 700-1400 cm^{-1} at St Denis and Maïdo are recorded with the same settings. Two maximum optical path difference (MOPD) of 82 and 125 cm are operated to gather the interferogram of the direct solar radiation, and then the interferogram is transformed to a spectrum with the spectral resolution of 0.010975 and 0.0072 cm^{-1} through a fast Fourier transform (FFT) algorithm. The HgCdTe (MCT) detector collects the spectrum and one specific interference filter is used to narrow the optical band to regions of interests in order to improve the signal-to-noise (SNR).

2.1   Retrieval strategy

We applied the SFIT4_v9.4.4 algorithm (Pougatchev et al., 1995) to retrieve information from the spectra: it simulates the spectrum observed by the ground-based FTIR and looks for the optimum state vector (the retrieved state) to minimize the residual between the simulated and the observed spectra. Table 1 lists the retrieval window, interfering gases, spectroscopic database, a priori profile, background parameters and SNR used in the SFIT4 algorithm for the SF_6 retrieval at St Denis and Maïdo, together with the obtained degrees of freedom of signal (DOFS).

2.1.1   Retrieval window

The broad unresolved Q branch of the ν_3 band of SF_6, at 947.9 cm^{-1} (Varanasi et al., 1992), is always used to retrieve SF_6 by remote sensing techniques. Zander et al. (1991) used 946.9-948.9 cm^{-1} to do the FTIR retrieval at Jungfraujoch and Krieg et al. (2005) used 947.2-948.6 cm^{-1} for Kitt Peak and Ny–Ålesund FTIR retrievals. We also used the SF_6 absorption line at 947.9 cm^{-1} and the retrieval window 946.5-949.0 cm^{-1} to perform the FTIR retrieval at Réunion Island. However, compared with the previous studies, our retrieval window contains an additional weak H_2O absorption line at 946.68 cm^{-1}. Since there is a strong H_2O absorption line at 948.26 cm^{-1} and a strong CO_2 line at 947.74 cm^{-1} (see Fig. 2), the SF_6 is inevitably influenced

3

by these two species, especially from H_2O due to its larger variability in the atmosphere. A better fitting of H_2O (with a smaller root mean square (RMS) of the fitting residual) is obtained by the larger retrieval window. In addition, to minimize interference from H_2O and CO_2, their profiles are retrieved simultaneously with the SF_6 profile.

2.1.2 Instrument line shape

In order to acquire the instrument line shape (ILS) and to verify the alignment of the instrument, daily HBr cell measurements are carried out automatically at both sites. The LINEFIT14.5 program (Hase et al., 1999) is applied to obtain the modulation and phase parameters of the ILS, which are used as an input in the SFIT4 algorithm. Note that, we made a 3-order polynomial fitting from the LINEFIT outputs, and then retrieved the polynomial parameters in SFIT4 algorithm for both modulation and phase.

2.1.3 Spectroscopy

The spectroscopy of SF_6 was taken from the Pseudo-line lists (http://mark4sun.jpl.nasa.gov/pseudo.html), and the spectroscopy of the other species was obtained from the ATM16 linelists (Toon, 2014). Pseudo-line lists were produced by Geoff Toon (NASA-JPL) by fitting all the laboratory spectra simultaneously, which includes mean intensities and effective lower state energies on a 0.005 cm^{-1} frequency grid. These artificial lines at arbitrary positions do not represent transitions of molecules. Instead, their line-widths and intensities are fitted to the laboratory spectra such that the pseudo-line lists allow to simulate the measured spectra.

2.1.4 A priori profile

To construct the a priori profile close to the true one, we used the US standard atmosphere (1976) SF_6 (National Geophysical Data Center, 1992) as the shape of the a priori profile, and then scaled it with one factor to make the concentration of the lowest level equal to the annual mean of SMO measurements in 2009. The H_2O a priori profile was derived from the 6-hourly NCEP reanalysis data. For the a priori profiles of the other interfering species (see Table 1), the mean of the Whole Atmosphere Community Climate Model (WACCM) version 6 monthly profiles between 1980 and 2020 were adopted.

2.1.5 Regularisation matrix

The a priori covariance matrix together with the measurement noise covariance matrix determine the weights of a priori knowledge and measurement information (Rodgers, 2000). The SNR were set as 180 and 400 at St Denis and Maïdo, respectively. In order to extract as much information as possible from the measurements and to avoid too many oscillations in the retrieved SF_6 profiles, we used 30% and 14% as the diagonal elements (the same value for all levels) to create the regularisation matrices at St Denis and Maïdo, respectively. The correlation width was set as 10.0 km. Note that the diagonal value of the regularisation matrix is a key parameter to balance the contribution from the measurement information and the a priori information, which does not represent the real variability of SF_6 in the atmosphere.

2.1.6 Averaging kernel

Figure 3 shows the typical averaging kernel of the SF_6 retrieval at Maïdo. The FTIR retrieval is sensitive to the altitude range from the surface to 20 km (the whole troposphere and lower stratosphere). The mean and standard deviation of the DOFS of the SF_6 retrievals is 1.0 ± 0.1 at St Denis and 1.1 ± 0.1 at Maïdo, indicating that the SF_6 retrievals have information content in only one individual layer (mainly 0-20 km) and have no profile information. That means the retrieved profiles are not reliable, and we should focus on the total column. In this study, the SF_6 retrievals at St Denis were combined with Maïdo retrievals to extend the time coverage for the trend in Sect. 3. The DOFS at the two stations are very close, and there is no observed trend in the time series of the DOFS.

2.2 Error budget

Based on the optimal estimation method (Rodgers, 2000), the difference between the retrieved state vector $\hat{x}$ and the true state vector x_t could be expressed as

$$\hat{x} - x_t = (\mathbf{A} - \mathbf{I})(x_t - x_a) + \mathbf{G}_y \mathbf{K}_b(b_t - b) + \mathbf{G}_y \triangle \mathbf{f} + \mathbf{G}_y \varepsilon_y, \tag{1}$$

where x_a is the a priori state vector; $\mathbf{A}$ is the averaging kernel matrix, representing the sensitivity of the retrieved state vector to the true state vector; $\mathbf{I}$ is a unit matrix; $\mathbf{G}_y$ is the contribution matrix, representing the sensitivity of the retrieval to the measurement y; $\mathbf{K}_b$ is the weight function, representing the sensitivity of the forward model $F(x, b)$ to the forward model parameters; b is the vector of forward model parameters that are not retrieved; b_t is the vector of true forward model parameters; $\triangle \mathbf{f}$ is the forward model systematic uncertainty; ε_y is the measurement noise covariance matrix. Note that the state vector x, which is the vector of forward model parameters that are retrieved, is a higher dimensional vector which components consist of the target SF_6 profile components, the concentration profiles for the interfering species (H_2O, CO_2) and other retrieval parameters (slope, ILS, ...).

The error on the target SF_6 profile is obtained by extracting the SF_6 components from the vectorial equation in Eq. 1. The error on the retrieved SF_6 profile $(\hat{x} - x_t)_{SF_6}$ then consists of the smoothing error $(\mathbf{A} - \mathbf{I})(x_t - x_a)$, model parameter error $\mathbf{G}_y \mathbf{K}_b(b_t - b)$, forward model error $\mathbf{G}_y \triangle \mathbf{f}$ and measurement noise $\mathbf{G}_y \varepsilon_y$. As the SFIT4 algorithm is well established and only the physics of the absorption is included in the transmission of radiation, the forward model error can be ignored.

For the smoothing error, except for the uncertainty from SF_6, it also includes the uncertainties from the H_2O profile, the CO_2 profile, the C_2H_4 and O_3 scaling factors and some other parameters (see Table 1), which is defined as retrieval parameter error ε_{re}. Since the absorption lines of H_2O and CO_2 are very strong in the retrieval window, the ε_{re} is separated into three components.

$$(\mathbf{A} - \mathbf{I})(x_t - x_a) = (\mathbf{A}_{SF6,SF6} - \mathbf{I})(x_{t,SF_6} - x_{a,SF_6}) + \varepsilon_{re} \tag{2}$$

$$\varepsilon_{re} = \mathbf{A}_{SF_6,H_2O}(x_{t,H_2O} - x_{a,H_2O}) + \mathbf{A}_{SF_6,CO_2}(x_{t,CO_2} - x_{a,CO_2})$$
$$+ \mathbf{A}_{SF_6,others}(x_{t,others} - x_{a,others}), \tag{3}$$

where $\mathbf{A}_{SF_6,SF_6}$, $\mathbf{A}_{SF_6,H_2O}$, $\mathbf{A}_{SF_6,CO_2}$ and $\mathbf{A}_{SF_6,others}$ are the matrices extracted from the full averaging kernel $\mathbf{A}$ by selecting the components $\mathbf{A}_{ij}$ where the row index i runs over all SF$_6$ components in the state vector $\boldsymbol{x}$ and the column index j runs over all SF$_6$, H$_2$O, CO$_2$ and other components in state vector $\boldsymbol{x}$. $\boldsymbol{x}_{t,SF_6}$ and $\boldsymbol{x}_{a,SF_6}$, $\boldsymbol{x}_{t,H_2O}$ and $\boldsymbol{x}_{a,H_2O}$, $\boldsymbol{x}_{t,CO_2}$ and $\boldsymbol{x}_{a,CO_2}$, $\boldsymbol{x}_{t,others}$ and $\boldsymbol{x}_{a,others}$ are the true and a priori values of SF$_6$, H$_2$O, CO$_2$ and other retrieval parameters, respectively.

Systematic and random components are considered to characterize the uncertainty of each parameter. For the smoothing error $(\mathbf{A}_{SF6,SF6} - \mathbf{I})(\boldsymbol{x}_{t,SF_6} - \boldsymbol{x}_{a,SF_6})$, we assumed that the systematic uncertainty of $\boldsymbol{\varepsilon}(\boldsymbol{x}_{t,SF_6} - \boldsymbol{x}_{a,SF_6})$ is 5% relative to the a priori profile ($\sigma_{SF6,ai} = 0.05x_{ai}$). Then, the diagonal and off-diagonal values of the systematic part of $\boldsymbol{\varepsilon}(\boldsymbol{x}_{t,SF_6} - \boldsymbol{x}_{a,SF_6})(\boldsymbol{x}_{t,SF_6} - \boldsymbol{x}_{a,SF_6})^T$ are calculated as ($\sigma_{SF6,ai}^2$) and $\sigma_{SF6,ai}\sigma_{SF6,aj}$, respectively (von Clarmann, 2014). The random part of $\boldsymbol{\varepsilon}(\boldsymbol{x}_{t,SF_6} - \boldsymbol{x}_{a,SF_6})(\boldsymbol{x}_{t,SF_6} - \boldsymbol{x}_{a,SF_6})^T$ is constructed same as the regularisation matrix but the diagonal elements were set as 30% for both St Denis and Maïdo. For the measurement error $\mathbf{G}_y\boldsymbol{\varepsilon}$, there is no systematic uncertainty and the random uncertainty is derived from SNR.

For the ε_{re}, we mainly focus on the influence from H$_2$O and CO$_2$. The systematic and random uncertainties of H$_2$O profile were derived from the bias and the standard deviation of the differences between the NCEP profiles and the balloon sondes. In general, the systematic uncertainty is about 5% and random uncertainty is about 10% from surface to 10 km. The CO$_2$ systematic uncertainty is assumed to be 5% of the average of the WACCM monthly profiles, and the random uncertainty is the standard deviation of the WACCM monthly profiles from 1980 to 2020.

For the model parameter error $\mathbf{G}_y\mathbf{K}_b(\boldsymbol{b}_t - \boldsymbol{b})$, we only show the significant parameters here, i.e. temperature, spectroscopy, solar zenith angle (SZA), ILS and zero level offset (zshift). The systematic and random uncertainties of the temperature profile were derived from the mean and the standard deviation of the differences between the NCEP profiles and the balloon sondes at Réunion Island in 2011. In general, the systematic bias is about 5 K below 10 km, 3 K between 10 km and 15 km and 1 K above 15 km. The standard deviation is about 2-4 K in troposphere and 5-10 K above tropopause height. The SF$_6$ spectroscopy uncertainty is from the Pseudo database, 2% for the systematic part and zero for the random part. 0.1% and 0.2% were adopted for the systematic and random uncertainties of SZA according to the Pysolar package (one Python code to calculate the solar position http://pysolar.org/). 5% and 1% were adopted for both systematic and random uncertainties of the ILS parameters and zshift, respectively.

Table 2 lists the SF$_6$ FTIR retrieval systematic and random uncertainties (%) at St Denis and Maïdo. The "retrieval parameters" in the Table 2 represents the "others" in Eq.3. The smoothing error, measurement error, H$_2$O interfering and temperature error at St Denis are much larger than those at Maïdo. In total, the retrieval systematic/random uncertainties (relative to the retrieved SF$_6$ total column) are 4.6%/14.0% at St Denis and 3.7%/6.7% at Maïdo, respectively.

3 SF$_6$ trend analysis

3.1 Data sets

3.1.1 SMO in-situ measurements

Since 1998, a four channel gas chromatograph (CATS) system has been measuring the surface SF$_6$ at the SMO site. Due to the high accuracy and precision, the CATS SF$_6$ daily data from the NOAA/ESRL halocarbons in situ measurement program is considered to be a reference for comparison with the FTIR retrievals. Note that these are daily medians data instead of daily means, in order to filter the higher outliers from local pollutions. As there is an improvement of the instrument in June 2000, the standard deviation of one-day's measurements decreased from 0.2-0.4 pptv to 0.02-0.04 pptv after the change (Hall et al., 2011).

3.1.2 MIPAS

MIPAS derived the global distributions of profiles of SF$_6$ from limb observations between 2002 and 2012. MIPAS observed spectra in full spectral resolution (FR) mode (spectral resolution: 0.05 cm^{-1}) and reduced resolution (RR) mode (spectral resolution: 0.121 cm^{-1}) before and after January 2005. In this paper, we used the latest SF$_6$ product with newly calibrated level 1b spectra (Haenel et al., 2015) to compare with the FTIR retrievals and to make the SF$_6$ trend analysis. The SF$_6$ data used here are version V5h_SF6_20 for the FR data product and V5r_SF6_222 and V5r_SF6_223 for the RR period. The MIPAS retrievals cover the upper troposphere (down to cloud top, or ∼6 km in cloud free cases) and the stratosphere only (about 55 km; see Fig. 7). Since MIPAS single SF$_6$ profiles are very noisy, we used the monthly means in the latitude band of 20-25° S.

3.1.3 ACE-FTS

Global distributions of SF$_6$ are also monitored by ACE-FTS occultation measurements from 2004 (Boone et al., 2013). We used the ACE-FTS level 2 version 3.5 monthly data (2004-2013) from the ACE/SCISAT database, and only the measurements without any known issues (quality flag = 0) were selected (Sheese et al., 2015). The ACE-FTS data has been validated with MkIV balloon profiles (Velazco et al., 2011). Since ACE-FTS mainly look at the polar area, there are few measurements in the tropical zone. Geller et al. (1997) found that SF$_6$ is well-mixed throughout the southern hemisphere, therefore, we enlarged the latitude band for ACE-FTS measurements to 0-40° S to get a robust result. Similar to MIPAS measurements, ACE-FTS collects the spectra in the upper troposphere and stratosphere (about 10-30 km; see Fig. 7).

3.1.4 Ground-based FTIR

As the FTIR SF$_6$ retrievals have only one-layer's information , we applied the dry air column-averaged SF$_6$ (X_{SF_6}) of FTIR measurements to quantitatively compare with other data sets. X_{SF_6} is obtained by dividing the SF$_6$ total column by the dry air

total column.

$$X_{SF_6} = \frac{TC_{SF_6}}{TC_{air}^{dry}}, \tag{4}$$

$$TC_{air}^{dry} = \frac{P_s}{gm_{air}^{dry}} - TC_{H_2O}(m_{H_2O}/m_{air}^{dry}), \tag{5}$$

where TC_{SF_6} and TC_{air}^{dry} are the total columns of SF$_6$ and dry air; P_s is the surface pressure; g is the acceleration of gravity depending on the latitude and altitude; m_{H_2O} and m_{air}^{dry} are the molecular mass of H$_2$O and dry air, respectively; TC_{H_2O} is the total column of H$_2$O from NCEP re-analysis data. The surface pressure is recorded by Vaisala PTB210 sensor, with the accuracy better than 0.1 hPa. The systematic uncertainty of H$_2$O in the troposphere is about 5%, and the TC_{H_2O} at Réunion Island is about 1-2 % of the TC_{air}. As a result, the uncertainty of the TC_{air}^{dry} is better than 0.1%.

Note that the SF$_6$ concentration is almost constant in the troposphere, but much lower in the stratosphere. Such a kind of profile will lead to a systematic bias if we combine the X_{SF_6} in 0-100 km (above St Denis) and X_{SF_6} in 2.155-100 km (above Maïdo) directly. To avoid such systematic bias, we kept the X_{SF_6} at St Denis unchanged and applied a scaling factor of 1.01 to the X_{SF_6} at Maïdo, which is the ratio of X_{SF_6} in 0-100 km to X_{SF_6} in 2.155-100 km based on the FTIR SF$_6$ a priori profile but scaled with the annual mean of SMO in-situ measurements in 2014.

Figure 4 shows the locations of the ground-based observations and the latitude bands covered by the satellites. The SF$_6$ time series of SMO in-situ, MIPAS and ACE-FTS measurements and FTIR retrievals at St Denis and Maïdo are presented in Fig. 5. For MIPAS, ACE-FTS and FTIR data, the errorbar is the standard deviation of all the measurements in one month. Since the FTIR retrieval has the largest sensitivity in the vertical range of 5-15 km (see Fig. 3), we selected the 11 km of MIPAS and 12.5 km of ACE-FTS here. In general, SF$_6$ from these data sets are in good agreement, as the difference between each two measurements is within the their uncertainties.

3.2 Methodology

A regression model (Weatherhead et al., 1998) is applied to derive the SF$_6$ linear long-term trend based on the measurements of FTIR daily means, SMO daily medians and satellites (MIPAS and ACE-FTS) monthly means.

$$\boldsymbol{Y(t)} = A_0 + A_1 \cdot \boldsymbol{t} + \sum_{k=1}^{3}(A_{2k}\cos(2k\pi\boldsymbol{t}) + A_{2k+1}\sin(2k\pi\boldsymbol{t})) + \boldsymbol{\varepsilon(t)}, \tag{6}$$

where $\boldsymbol{Y(t)}$ is measurements with the $\boldsymbol{t}$ in fraction of year; A_0 is the intercept; A_1 is the annual growth; A_2 to A_7 are the periodic variations, mainly representing the seasonal cycle; $\varepsilon(\boldsymbol{t})$ is the residual between the measurements and the fitting model. To estimate the trend error σ_c, the auto-correlation of the residual should be taken into account (Santer et al., 2000).

$$\sigma_c = \sigma_d \frac{(n-2)}{[n(1-r)/(1+r)-2]}, \tag{7}$$

where σ_d is the regression error; n is the number of measurements; r is the lag-1 (one month) auto-correlation coefficient of the regression residuals.

3.3 Annual change

Figure 6 shows the SF_6 trends from the SMO in-situ measurements, the ground-based FTIR retrievals, the MIPAS measurements in the latitude band of 20-25° S for different altitudes (9-52 km), and the ACE-FTS measurements in the latitude band of 0-40° S for altitude range of 10.5-32.5 km. The vertical sensitivity of the FTIR retrieval is between surface and 20 km (see Fig. 3). For MIPAS and ACE-FTS measurements, Fig. 6 also shows the number of monthly means used for the trend analysis at each altitude (dotted lines). The annual growth of FTIR measurements is 0.265±0.013 pptv/year from 2004 to 2016, which is slightly weaker than the trend of the SMO in-situ measurements (0.285±0.002 pptv/year) for the same time period. Waugh et al. (2013) pointed out that the age of near-surface SF_6 at SMO (14°S) is about 0.4 years higher than that at Réunion Island (21°S). In addition, the global surface in-situ measurement network (https://www.esrl.noaa.gov/gmd/hats/combined/SF6.html) shows that the growth rate of SF_6 is slightly increasing with time. Therefore, it is acceptable that the trends from FTIR measurements at Réunion Island is slightly weaker than that from the SMO in-situ measurements.

The trend uncertainty from MIPAS data is less than the ACE-FTS data and the FTIR retrievals because MIPAS has many more data points. The profile of SF_6 trend shows a peak in 11-13 km altitude from the MIPAS measurements, and a peak in 11.5-16.5 km from the ACE-FTS measurements. As the SF_6 emissions are all at Earth's surface and there is almost no removal mechanism in the troposphere and stratosphere (Kovács et al., 2017), the SF_6 concentration should be well-mixed in the troposphere (the tropopause height above Réunion Island is about 16.5 km) and decreasing above the tropopause, which was confirmed by the airborne in-situ measurements (Patra et al., 1997). Fig. 7 shows the SF_6 monthly means and the number of measurements in each month from MIPAS and ACE-FTS. The numbers of good quality measurements at 9 km for MIPAS and 10.5 km for ACE-FTS are considerably reduced because a large number of measurements are contaminated by clouds. As a consequence, the trends at these altitudes from MIPAS and ACE-FTS were derived from a small number of measurements, leading to larger uncertainties. For example, in October 2004, there are only 3 ACE-FTS measurements within the latitude band range 0-40° S, and the SF_6 monthly mean at 10.5 km is 7.57 pptv, which is very large compared with the monthly means nearby in time (the SF_6 monthly means at 10.5 km in November and December are 4.92 and 5.80 pptv).

In general, the SF_6 trend from the SMO in-situ measurements at surface or from the FTIR retrievals is close to the trends at the troposphere from the MIPAS and ACE-FTS measurements. In the stratosphere, satellite measurements (both MIPAS and ACE-FTS) show that the SF_6 trend decreases with increasing altitude. The change of the SF_6 trends in the stratosphere could be applied to estimate how long it takes for the well-mixed air mass to transport from surface to the high altitude in a large scale (Waugh, 2002; Stiller et al., 2012).

4 Conclusions

The SF_6 total columns were retrieved with SFIT4 algorithm from two FTIRs at Réunion Island (21°S, 55°E) in 2004-2016. The FTIR SF_6 retrieval is sensitive to the whole troposphere and lower stratosphere, but has only one degree of freedom. We used the retrieval window (946.5-949.0 cm^{-1}) to do the SF_6 retrieval at St Denis and Maïdo, with the broad unresolved Q branch of the ν_3 band of SF_6, at 947.9 cm^{-1}. Nearby are a strong H_2O absorption line at 948.26 cm^{-1}, a weak H_2O absorption line at

9

946.68 cm^{-1} and a strong CO_2 line at 947.74 cm^{-1}. The SF$_6$ retrieval product is influenced by these two species, especially by H$_2$O due to its larger variability in the atmosphere. The retrieval window in this study is wider than the previous ones (Zander et al., 1991; Krieg et al., 2005) because for the humid sites, such as St Denis, a better fitting is obtained with the larger window.

To estimate the SF$_6$ retrieval error, four components (the smoothing error, forward model parameter error, measurement error and other retrieval parameter errors) have been discussed in detail. In total, the systematic/random uncertainties of the FTIR retrieved SF$_6$ columns are 4.6%/14.0% at St Denis and 3.7%/6.7% at Maïdo. Both systematic/random uncertainties at St Denis are larger than those at Maïdo, because of the lower SNR and the higher water vapour abundance at St Denis.

The trend of X_{SF_6} derived from FTIR measurements is 0.265±0.013 pptv/year for 2004-2016, which is slightly weaker than the trend from the SMO in-situ measurements (0.285±0.002 pptv/year) for the same time period. The SF$_6$ trends at 9 km from MIPAS measurements and 10.5 km from ACE-FTS measurements are rather uncertain due to scarceness of data, because the MIPAS and ACE-FTS measurements are contaminated by cumulus clouds at low altitudes and these values are not included for the trend calculation. The SF$_6$ trends in the troposphere from both MIPAS and ACE-FTS measurements are close to the trends from FTIR retrievals and SMO in-situ measurements; the SF$_6$ trends from MIPAS and ACE-FTS above the tropopause height decrease with increasing altitude.

5 Data availability

The FTIR SF$_6$ retrievals at Réunion Island (St Denis and Maïdo) are not public available yet. To obtain access to site data, please contact the author or the BIRA-IASB FTIR group. The MIPAS SF$_6$ data is provided by the MIPAS satellite group at KIT/IMK, please contact Gabriele Stiller (gabriele.stiller@kit.edu). The ACE-FTS data used in this study are available from http://ace.uwaterloo.ca/data/ (registration required). SMO in-situ SF$_6$ measurements are publicly available ftp://ftp.cmdl.noaa.gov/hats/sf6/insituGCs/CATS/daily/.

References

Bernath, P.: The Atmospheric Chemistry Experiment (ACE), J. Quant. Spectrosc. Radiat. Transf., 186, 3–16, doi:10.1016/j.jqsrt.2016.04.006, 2017.

Bernath, P. F., McElroy, C. T., Abrams, M. C., Boone, C. D., Butler, M., Camy-Peyret, C., Carleer, M., Clerbaux, C., Coheur, P. F., Colin, R., DeCola, P., DeMazière, M., Drummond, J. R., Dufour, D., Evans, W. F. J., Fast, H., Fussen, D., Gilbert, K., Jennings, D. E., Llewellyn, E. J., Lowe, R. P., Mahieu, E., McConnell, J. C., McHugh, M., McLeod, S. D., Michaud, R., Midwinter, C., Nassar, R., Nichitiu, F., Nowlan, C., Rinsland, C. P., Rochon, Y. J., Rowlands, N., Semeniuk, K., Simon, P., Skelton, R., Sloan, J. J., Soucy, M. A., Strong, K., Tremblay, P., Turnbull, D., Walker, K. A., Walkty, I., Wardle, D. A., Wehrle, V., Zander, R., and Zou, J.: Atmospheric chemistry experiment (ACE): Mission overview, doi:10.1029/2005GL022386, 2005.

Boone, C. D., Walker, K. A., and Bernath, P. F.: Version 3 Retrievals for the Atmospheric Chemistry Experiment Fourier Transform Spectrometer (ACE-FTS), in: The Atmospheric Chemistry Experiment ACE at 10: A Solar Occultation Anthology, JA. Deepak Publishing 2013, Hampton, Virginia, USA, p. 103–127, 2013.

Engel, A.: Temporal development of total chlorine in the high-latitude stratosphere based on reference distributions of mean age derived from CO2 and SF6, J. Geophys. Res., 107, 4136, doi:10.1029/2001JD000584, 2002.

Geller, L. S., Elkins, J. W., Lobert, J. M., Clarke, A. D., Hurst, D. F., Butler, J. H., and Myers, R. C.: Tropospheric SF_6 : Observed latitudinal distribution and trends, derived emissions and interhemispheric exchange time, Geophys. Res. Lett., 24, 675–678, doi:10.1029/97GL00523, 1997.

Haenel, F. J., Stiller, G. P., von Clarmann, T., Funke, B., Eckert, E., Glatthor, N., Grabowski, U., Kellmann, S., Kiefer, M., Linden, A., and Reddmann, T.: Reassessment of MIPAS age of air trends and variability, Atmos. Chem. Phys., 15, 13 161–13 176, doi:10.5194/acp-15-13161-2015, 2015.

Hall, B. D., Dutton, G. S., Mondeel, D. J., Nance, J. D., Rigby, M., Butler, J. H., Moore, F. L., Hurst, D. F., and Elkins, J. W.: Improving measurements of SF_6 for the study of atmospheric transport and emissions, Atmos. Meas. Tech., 4, doi:10.5194/amt-4-2441-2011, 2011.

Hase, F., Blumenstock, T., and Paton-Walsh, C.: Analysis of the Instrumental Line Shape of High-Resolution Fourier Transform IR Spectrometers with Gas Cell Measurements and New Retrieval Software, Appl. Opt., 38, 3417, doi:10.1364/AO.38.003417, 1999.

Hase, F., Hannigan, J. W., Coffey, M. T., Goldman, A., Höpfner, M., Jones, N. B., Rinsland, C. P., and Wood, S. W.: Intercomparison of retrieval codes used for the analysis of high-resolution, ground-based FTIR measurements, J. Quant. Spectrosc. Radiat. Transf., doi:10.1016/j.jqsrt.2003.12.008, 2004.

Kovács, T., Feng, W., Totterdill, A., Plane, J. M. C., Dhomse, S., Gómez-Martín, J. C., Stiller, G. P., Haenel, F. J., Smith, C., Forster, P. M., García, R. R., Marsh, D. R., and Chipperfield, M. P.: Determination of the atmospheric lifetime and global warming potential of sulfur hexafluoride using a three-dimensional model, Atmos. Chem. Phys., 17, 883–898, doi:10.5194/acp-17-883-2017, 2017.

Krieg, J., Nothholt, J., Mahieu, E., Rinsland, C. P., and Zander, R.: Sulphur hexafluoride (SF6): Comparison of FTIR-measurements at three sites and determination of its trend in the northern hemisphere, J. Quant. Spectrosc. Radiat. Transf., 92, 383–392, doi:10.1016/j.jqsrt.2004.08.005, 2005.

Levin, I., Naegler, T., Heinz, R., Osusko, D., Cuevas, E., Engel, A., Ilmberger, J., Langenfelds, R. L., Neininger, B., Rohden, C. V., Steele, L. P., Weller, R., Worthy, D. E., and Zimov, S. a.: The global SF6 source inferred from long-term high precision atmospheric measurements and its comparison with emission inventories, Atmos. Chem. Phys., 10, 2655–2662, doi:10.5194/acp-10-2655-2010, 2010.

11

Maiss, M. and Brenninkmeijer, C. A. M.: Atmospheric SF6: Trends, sources, and prospects, Environ. Sci. Technol., 32, 3077–3086, doi:10.1021/es9802807, 1998.

Maiss, M. and Levin, I.: Global increase of SF6 observed in the atmosphere, Geophys. Res. Lett., 21, 569–572, doi:10.1029/94GL00179, 1994.

5   Mieville, A., Granier, C., Liousse, C., Guillaume, B., Mouillot, F., Lamarque, J. F., Grégoire, J. M., and Pétron, G.: Emissions of gases and particles from biomass burning during the 20th century using satellite data and an historical reconstruction, Atmos. Environ., doi:10.1016/j.atmosenv.2010.01.011, 2010.

Moss, R. H., Edmonds, J. A., Hibbard, K. A., Manning, M. R., Rose, S. K., van Vuuren, D. P., Carter, T. R., Emori, S., Kainuma, M., Kram, T., Meehl, G. A., Mitchell, J. F. B., Nakicenovic, N., Riahi, K., Smith, S. J., Stouffer, R. J., Thomson, A. M., Weyant, J. P., and Wilbanks,

10 T. J.: The next generation of scenarios for climate change research and assessment, Nature, 463, 747–756, doi:10.1038/nature08823, 2010.

National Geophysical Data Center: U.S. standard atmosphere (1976), Planet. Space Sci., 40, 553–554, doi:10.1016/0032-0633(92)90203-Z, 1992.

Patra, P. K., Lal, S., Subbaraya, B. H., Jackman, C. H., and Rajaratnam, P.: Observed vertical profile of sulphur hexafluoride (SF6) and its atmospheric applications, J. Geophys. Res. Atmos., 102, 8855–8859, doi:10.1029/96JD03503, 1997.

15 Patra, P. K., Takigawa, M., Dutton, G. S., Uhse, K., Ishijima, K., Lintner, B. R., Miyazaki, K., and Elkins, J. W.: Transport mechanisms for synoptic, seasonal and interannual SF6 variations and "age" of air in troposphere, Atmos. Chem. Phys., 9, 1209–1225, doi:10.5194/acp-9-1209-2009, 2009.

Pougatchev, N. S., Connor, B. J., and Rinsland, C. P.: Infrared measurements of the ozone vertical distribution above Kitt Peak, J. Geophys. Res., 100, 16 689, doi:10.1029/95JD01296, 1995.

20 Ray, E. A., Moore, F. L., Elkins, J. W., Rosenlof, K. H., Laube, J. C., Röckmann, T., Marsh, D. R., and Andrews, A. E.: Quantification of the SF 6 lifetime based on mesospheric loss measured in the stratospheric polar vortex, J. Geophys. Res. Atmos., 122, 4626–4638, doi:10.1002/2016JD026198, 2017.

Rigby, M., Mühle, J., Miller, B. R., Prinn, R. G., Krummel, P. B., Steele, L. P., Fraser, P. J., Salameh, P. K., Harth, C. M., Weiss, R. F., Greally, B. R., O'Doherty, S., Simmonds, P. G., Vollmer, M. K., Reimann, S., Kim, J., Kim, K.-R., Wang, H. J., Olivier, J. G. J., Dlugokencky, E. J.,

25 Dutton, G. S., Hall, B. D., and Elkins, J. W.: History of atmospheric SF6 from 1973 to 2008, Atmos. Chem. Phys., 10, 10 305–10 320, doi:10.5194/acp-10-10305-2010, 2010.

Rinsland, C. P., Brown, L. R., and Farmer, C. B.: Infrared spectroscopic detection of sulfur hexafluoride (sf6) in the lower stratosphere and upper troposphere, J. Geophys. Res., 95, 5577, doi:10.1029/JD095iD05p05577, 1990.

Rinsland, C. P., Goldman, A., Stephen, T. M., Chiou, L. S., Mahieu, E., and Zander, R.: SF6 ground-based infrared solar absorption mea-

30 surements: Long-term trend, pollution events, and a search for SF5CF3 absorption, J. Quant. Spectrosc. Radiat. Transf., 78, 41–53, doi:10.1016/S0022-4073(02)00177-2, 2003.

Rodgers, C. D.: Inverse Methods for Atmospheric Sounding - Theory and Practice, vol. 2, World scientific, doi:10.1142/9789812813718, 2000.

Santer, B. D., Wigley, T. M. L., Boyle, J. S., Gaffen, D. J., Hnilo, J. J., Nychka, D., Parker, D. E., and Taylor, K. E.: Statistical signifi-

35 cance of trends and trend differences in layer-average atmospheric temperature time series, J. Geophys. Res. Atmos., 105, 7337–7356, doi:10.1029/1999JD901105, 2000.

Schultz, M. G., Heil, A., Hoelzemann, J. J., Spessa, A., Thonicke, K., Goldammer, J. G., Held, A. C., Pereira, J. M. C., and van Het Bolscher, M.: Global wildland fire emissions from 1960 to 2000, Global Biogeochem. Cycles, doi:10.1029/2007GB003031, 2008.

Sheese, P. E., Boone, C. D., and Walker, K. A.: Detecting physically unrealistic outliers in ACE-FTS atmospheric measurements, Atmos. Meas. Tech., 8, 741–750, doi:10.5194/amt-8-741-2015, 2015.

Stiller, G. P., von Clarmann, T., Höpfner, M., Glatthor, N., Grabowski, U., Kellmann, S., Kleinert, A., Linden, A., Milz, M., Reddmann, T., Steck, T., Fischer, H., Funke, B., López-Puertas, M., and Engel, A.: Global distribution of mean age of stratospheric air from MIPAS SF6 measurements, Atmos. Chem. Phys., 8, 677–695, doi:10.5194/acp-8-677-2008, 2008.

Stiller, G. P., von Clarmann, T., Haenel, F., Funke, B., Glatthor, N., Grabowski, U., Kellmann, S., Kiefer, M., Linden, A., Lossow, S., and López-Puertas, M.: Observed temporal evolution of global mean age of stratospheric air for the 2002 to 2010 period, Atmos. Chem. Phys., 12, 3311–3331, doi:10.5194/acp-12-3311-2012, 2012.

Toon, G. C.: Telluric line list for GGG2014, TCCON data archive, hosted by the Carbon Dioxide Information Analysis Center, Oak Ridge National Laboratory, Oak Ridge, Tennessee, U.S.A., doi:10.14291/tccon.ggg2014.atm.R0/1221656, 2014.

Varanasi, P., Gopalan, A., and Brannon, J.: Infrared absorption-coefficient data on SF6 applicable to atmospheric remote sensing, J. Quant. Spectrosc. Radiat. Transf., 48, 141–145, doi:10.1016/0022-4073(92)90083-G, 1992.

Velazco, V. A., Toon, G. C., Blavier, J.-F. L., Kleinböhl, A., Manney, G. L., Daffer, W. H., Bernath, P. F., Walker, K. A., and Boone, C.: Validation of the Atmospheric Chemistry Experiment by noncoincident MkIV balloon profiles, J. Geophys. Res. Atmos., 116, D06 306, doi:10.1029/2010JD014928, 2011.

von Clarmann, T.: Smoothing error pitfalls, Atmos. Meas. Tech., 7, 3023–3034, doi:10.5194/amt-7-3023-2014, 2014.

Waugh, D.: Age of stratospheric air: Theory, observations, and models, Rev. Geophys., 40, 1010, doi:10.1029/2000RG000101, 2002.

Waugh, D. W., Crotwell, A. M., Dlugokencky, E. J., Dutton, G. S., Elkins, J. W., Hall, B. D., Hintsa, E. J., Hurst, D. F., Montzka, S. A., Mondeel, D. J., Moore, F. L., Nance, J. D., Ray, E. A., Steenrod, S. D., Strahan, S. E., and Sweeney, C.: Tropospheric SF6 : Age of air from the Northern Hemisphere midlatitude surface, J. Geophys. Res. Atmos., 118, 11,429–11,441, doi:10.1002/jgrd.50848, 2013.

Weatherhead, E. C., Reinsel, G. C., Tiao, G. C., Meng, X.-L., Choi, D., Cheang, W.-K., Keller, T., DeLuisi, J., Wuebbles, D. J., Kerr, J. B., Miller, A. J., Oltmans, S. J., and Frederick, J. E.: Factors affecting the detection of trends: Statistical considerations and applications to environmental data, J. Geophys. Res. Atmos., 103, 17 149–17 161, doi:10.1029/98JD00995, 1998.

WMO: Scientific Assessment of Ozone Depletion: 2014, 55, 2014.

Zander, R., Rinsland, C. P., and Demoulin, P.: Infrared spectroscopic measurements of the vertical column abundance of sulfur hexafluoride, SF6 , from the ground, J. Geophys. Res., 96, 15 447, doi:10.1029/91JD01214, 1991.

Zhou, M., Vigouroux, C., Langerock, B., Wang, P., Dutton, G., Hermans, C., Kumps, N., Metzger, J.-M., Toon, G., and De Mazière, M.: CFC-11, CFC-12 and HCFC-22 ground-based remote sensing FTIR measurements at Réunion Island and comparisons with MIPAS/ENVISAT data, Atmos. Meas. Tech., 9, 5621–5636, doi:10.5194/amt-9-5621-2016, 2016.

Table 1. The retrieval window, interfering gases, spectroscopic database, a priori profile, background parameters (slope and zshift) and SNR used in SFIT4 algorithm for FTIR SF_6 retrieval at St Denis and Maïdo, together with the achieved DOFS (mean and the standard deviation) of the retrievals.

Target gas	SF_6
Window (cm^{-1})	946.5–949.0
Profile retrieval	SF_6, H_2O, CO_2
Column retrieval	C_2H_4, O_3
Spectroscopy	Pseudo, ATM16
A priori profile	US standard but scaled to SMO measurements
ILS	LINEFIT14.5
Background (St Denis/Maïdo)	slope, zshift/slope
SNR (St Denis/Maïdo)	180/400
DOFS (St Denis/Maïdo)	$1.0 \pm 0.1/1.1 \pm 0.1$

Table 2. The systematic and random uncertainties for the FTIR retrieved total column (%) at St Denis and Maïdo. σ_b are the relative systematic (random) uncertainties of the non-retrieved parameters (%). The "retrieval parameters" represents the "others" in Eq.3. The SF_6 spectroscopy uncertainty is from the Pseudo-line database. When a relative uncertainty is smaller than 0.1 %, it is considered negligible and represented as "–".

Error	σ_b	St Denis Systematic	St Denis Random	Maïdo Systematic	Maïdo Random
Smoothing		0.1	6.3	0.1	3.0
Measurement		–	10.6	–	4.8
Retrieval parameters		0.2	–	0.1	0.1
H_2O interfering		0.4	6.1	1.0	3.3
CO_2 interfering		–	0.2	–	0.1
Temperature		4.1	2.0	2.5	1.0
SF_6 spectroscopy	2(0)	2.2	–	2.2	–
SZA	0.1(0.2)	0.2	0.4	0.3	0.6
ILS	5(5)	0.2	0.2	0.2	0.2
zshift	1(1)	0.2	0.2	–	–
Total		4.6	14.0	3.7	6.7

Figure 1. Time series of historical and projected global SF_6 emissions. Historical data cover 1900–2005 (black), and projections for the 2005–2100 time period correspond to four 4 RCP scenarios with 2.6, 4.5, 6.0 and 8.5 W/m² radiative forcing in 2100 relative to pre-industrial values (Moss et al., 2010). The black dot is the annual growth of SF_6 in 2012 according to the WMO report (WMO, 2014).
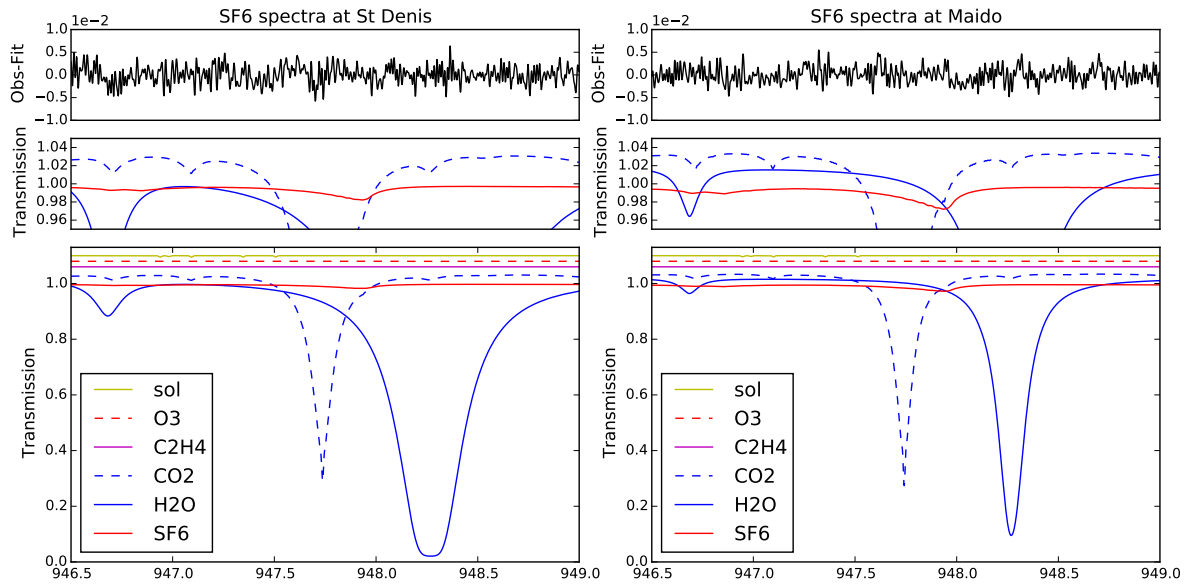

Figure 2. The typical spectrum of SF_6 retrieval microwindow (946.5-949.0 cm^{-1}) at St Denis (left) and Maïdo (right). The bottom panels list the absorption contribution from each species. To clarify the absorption lines, the transmittance is shifted by 0.02 for each species and the solar (sol) line list. The middle panels only show the transmittance between 0.95 and 1.05 to identify the SF_6 absorption line. The top panels show the transmittance residual (observed-calculated).
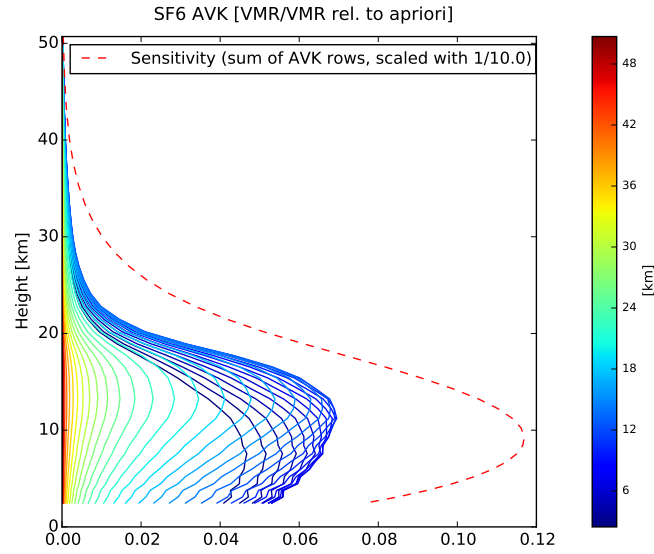
16

Figure 3. The typical averaging kernel of SF$_6$ retrieval at Maïdo. The solid lines represent the sensitivities at specific altitudes. The red dashed line is the sum of the row of averaging kernel scaled by 0.1, indicating the vertical sensitivity.
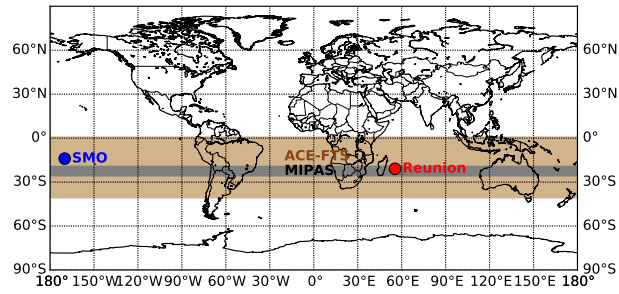

Figure 4. The locations of the ground-based sites (Réunion Island and SMO) as well as the latitude bands covered by the satellites (MIPAS and ACE-FTS).
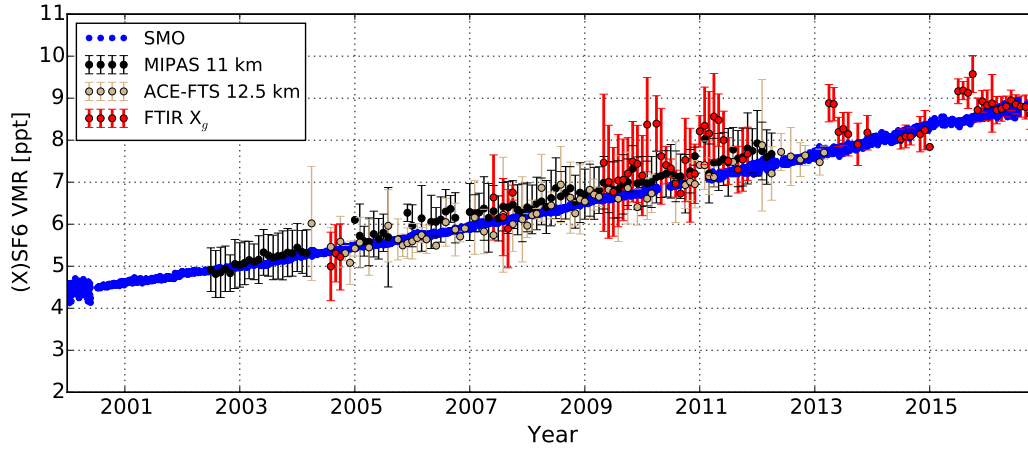
Figure 5. Time series of SMO in-situ SF_6 daily median (blue), MIPAS SF_6 monthly mean (20-25° S) at 11 km (black), ACE-FTS SF_6 monthly mean (0-40° S) at 12.5 km and FTIR X_{SF_6} monthly mean at St Denis and Maïdo (red). For MIPAS, ACE-FTS and ground-based FTIR measurements, the errorbar is the standard deviation within one month.
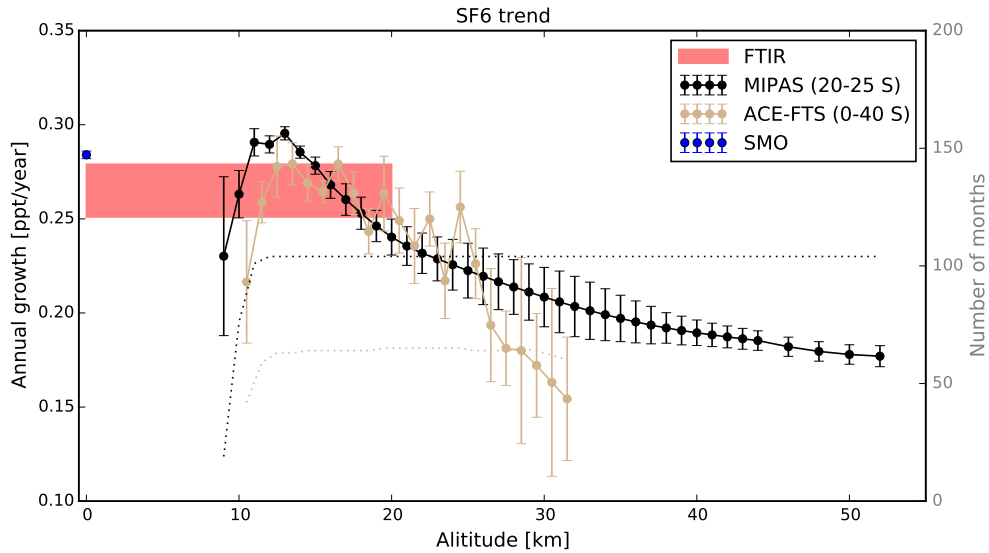

Figure 6. SF_6 annual growths from SMO in-situ measurements (2004-2016) (blue bar), ground-based FTIR measurements (2004-2016: combined St Denis and Maïdo)(pink bar), MIPAS measurements (2002-2012) in the latitude band of 20-25° S for different altitudes (9-52 km) (black solid line) and ACE-FTS measurements (2004-2013) in the latitude band of 0-40° S for altitude range of 10.5-32.5 km (brown solid line). For MIPAS and ACE-FTS measurements, the dotted line of the same colour is the number of monthly means used for trend analysis at each altitude.
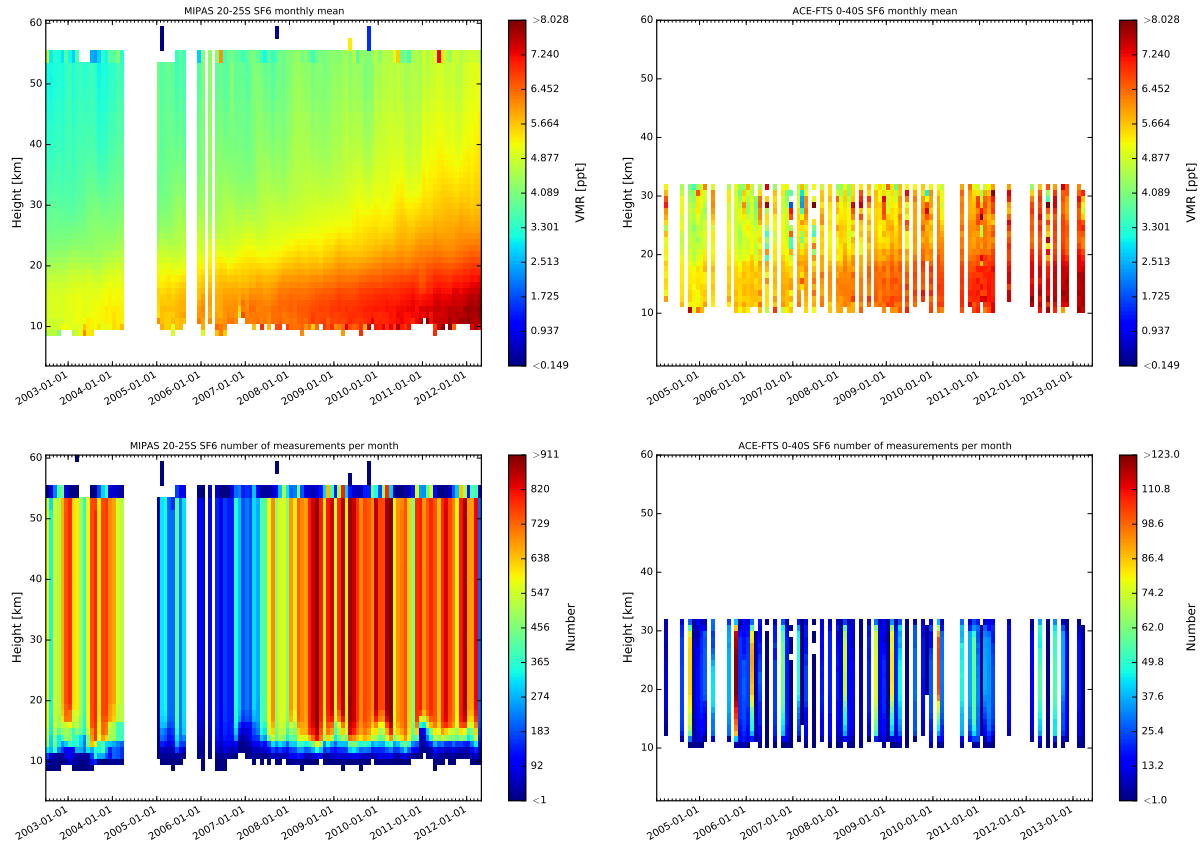
Figure 7. SF$_6$ monthly means of volume mixing ratios profiles (upper) and the number of measurements in each month (bottom) for MIPAS in the latitude band between 20-25° S (left) and ACE-FTS in the latitude band between 0-40° S (right).